Emerging trends in the sea state of the Beaufort and Chukchi seas

ONR Arctic Sea State DRI team:
Jim Thomson, Yalin Fan, Sharon Stammerjohn, Justin Stopa, W. Erick Rogers, Fanny Girard-Ardhuin, Fabrice Ardhuin, Hayley Shen, Will Perrie, Hui Shen, Steve Ackley, Alex Babanin, Qingxiang Liu, Peter Guest, Ted Maksym, Peter Wadhams, Chris Fairall, Ola Persson, Martin Doble, Hans Graber, Bjoern Lund, Vernon Squire, Johannes Gemmrich, Susanne Lehner, Benjamin Holt, Mike Meylan, John Brozena, and Jean-Raymond Bidlot

Correspondence: Jim Thomson, University of Washington, Applied Physics Laboratory, jthomson@apl.uw.edu, 206-616-0858

Abstract

The sea state of the Beaufort and Chukchi seas is controlled by the wind forcing and the amount of ice-free water available to generate surface waves. Clear trends in the annual duration of the open water season and in the extent of the seasonal sea ice minimum suggest that the sea state should be increasing, independent of changes in the wind forcing. Wave model hindcasts from four selected years spanning recent conditions are consistent with this expectation. In particular, larger waves are more common in years with less summer sea ice and/or a longer open water season, and peak wave periods are generally longer. The increase in wave energy may affect both the coastal zones and the remaining summer ice pack, as well as delay the autumn ice-edge advance. However, trends in the amount of wave energy impinging on the ice-edge are inconclusive, and the associated processes, especially in the autumn period of new ice formation, have yet to be well-described by in situ observations. There is an implicit trend and evidence for increasing wave energy along the coast of northern Alaska, and this coastal signal is corroborated by satellite altimeter estimates of wave energy.

Keywords: sea ice, Arctic Ocean, ocean surface waves

---

1. Introduction

The extent of seasonal sea ice in the Beaufort and Chukchi Sea of the Arctic Ocean is changing (Jeffries et al., 2013). This paper explores the timing and location of the annual ice minimum and transition to refreezing conditions, with application to the sea state over the open water portion of the domain. The sea state is set by the wind forcing, the open water fetch distance available for wave generation, and the duration of time over which the waves can accumulate energy from the wind. The wind forcing is episodic, and thus best interpreted as probabilities for events (i.e., storms). The open water distance, by contrast, has a much smoother signal that is dominated by the seasonal retreat and advance of the sea ice. It is the combination of these signals that determines the sea state of the Beaufort and Chukchi seas.

Trends in the Arctic sea ice have been examined by many previous studies (e.g., Wadhams, 1990; Wadhams and Davis, 2000; Stroeve et al., 2005, 2008; Simmonds and Keay, 2009; Kwok and Untersteiner, 2011). Meier et al. (2013) show that in recent decades the Arctic sea ice cover has thinned and become more seasonal, such that the total area covered is nearly 30% less at the annual minimum than the corresponding mean from 1979 to 2000. Stammerjohn et al. (2012) show that the duration of the summer open water season since 1979 has become much longer in the Beaufort and Chukchi seas due to an approximately 1.6 months earlier ice-edge retreat in spring, followed by an approximately 1.4 month later ice-edge advance in autumn. Stammerjohn et al. (2012) also find inter-annual links to the reduced ice extent which are attributed to heat fluxes, especially increased duration of summer solar heating, coupled with an overall thinner ice cover.

Coincident with the delay in the timing of the autumn ice advance, there is a trend towards stronger autumn storms in recent years (Serreze et al., 1993, 2001; Zhang et al., 2004). The combination of these winds and increased open water distances is expected to create high sea states (Francis et al., 2011; Francis and Vavrus, 2012; Vermaire et al., 2013; Thomson and Rogers, 2014) and increase air-sea fluxes of heat and momentum, particularly in the Beaufort and Chukchi seas (e.g., Simmonds and Keay, 2009). Some studies have connected reduced ice cover with specific storm activity, such as in August 2012 (Simmonds and Keay, 2012; Zhang et al., 2013; Parkinson and Comiso, 2013). Of these, Parkinson and Comiso (2013) conclude that the storm reduced the September ice extent minimum by an additional 5 percent. This relatively small effect suggests that high sea states may be the result of diminishing sea ice, but that high sea states are not yet the leading cause of diminishing sea ice.

However, there is some evidence for feedbacks between ocean surface waves and the loss of sea ice (e.g., Asplin et al., 2012). There are also feedbacks between waves and ice formation, such as the rapid freezing that occurs when waves cause pancake ice to develop (Wadhams et al., 1987; Lange et al., 1989). Waves are both associated with the formation of pancakes and attenuated by the pancakes, such that large areas of the ocean can freeze quickly. Although this process is typically associated with the Antarctic ice-edge or the Eastern Arctic, it is possible that this process will become important in the Beaufort and Chukchi seas of the Western Arctic. For example, this process is already common in the Sea of Okhotsk, which is relatively sheltered.

Here, we set aside the many interesting questions of wave-ice interactions (e.g., Squire et al., 1995; Squire, 2007) and focus instead on the large-scale patterns of the sea state in the Beaufort and Chukchi seas. In particular, we examine emerging trends in the probability of high sea states in the Beaufort and Chukchi seas. The recent work of Wang et al. (2015) indicate the wave heights are increasing slightly and wave periods are increasing strongly as a result of reductions in ice cover (as opposed to changes in the winds). We examine these trends and the autumn ice advance stage in particular. Section 2 describes the data products and model hindcasts used for the analysis. Section 3 presents the results, using a full climatology of ice products and a sub-set of wave hindcasts. Section 4 discusses the findings and corroborates the coastal signal with satellite altimeter estimates of wave trends. Section 5 concludes.

2. Methods

Analysis of ice and sea state trends uses satellite products and model hindcasts from an area-preserving domain shown in Figure 1. The domain is a rectangle which is constant in area with latitude, such that the range of longitudes included must expand northwards. The domain is selected to cover the full extent of the seasonal variation in sea ice cover from the middle of the summer (1 August) to the late autumn (31 October). The analysis that follows uses this rectangle and is restricted to the months of August, September, and October.

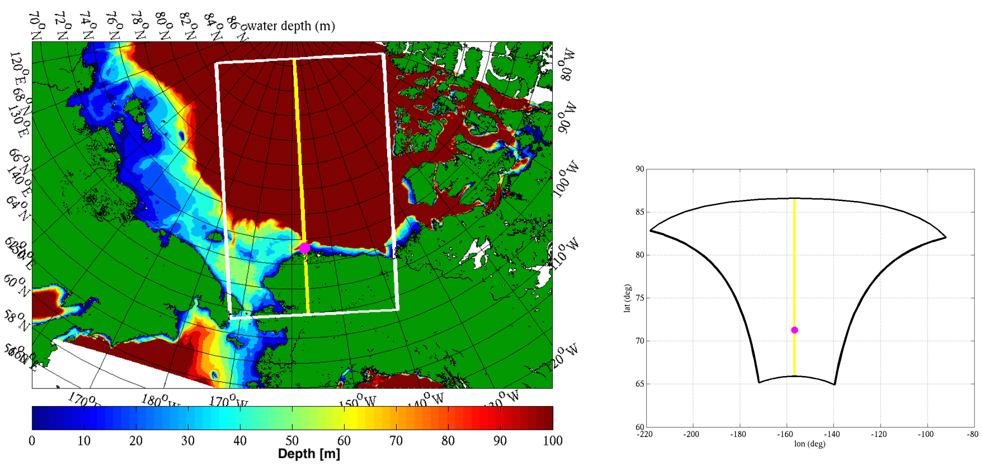

Figure 1: Region of analysis. (a) Map of bathymetry and the area-preserving rectangle defining the domain. Green colors show land. (b) Projection of the domain in latitude and longitude.

2.1. Sea ice satellite products

The analysis of sea ice area coverage used the NASA Goddard Space Flight Center (GSFC) Bootstrap SMMR-SSM/I Version 2 quasi-daily time series (1979 to 2014) of sea ice concentration from the EOS Distributed Active Archive Center (DAAC) at the National Snow and Ice Data Center (NSIDC, University of Colorado at Boulder, http://nsidc.org). The day of autumn ice advance and spring retreat is identified for each gridded (25 by 25 km pixel) location and for each sea ice year that begins/ends during the mean summer sea ice minimum (from mid-September to mid-September). When identifying day of ice-edge advance and retreat, an annual search window is defined such that it begins and ends during the mean summer sea ice extent minimum in mid-September. Within this interval, the year day of ice-edge advance is identified as when sea ice concentration first exceeds 15% (i.e., the approximate ice-edge) for at least five days. See Stammerjohn et al. (2012) and Comiso (2000, updated 2015, 2010) for further details.

Sea ice type was estimated by scatterometer, following **?** and **?**, with the goal of examining trends in the relative amounts of first-year ice versus multi-year ice. The sea ice type results are similar using the Envisat altimeter, following Tran et al. (2009).

2.2. Wind reanalysis product

The wind and ice product used for wave hindcasting is ERA-Interim, which is a global reanalysis of recorded climate observations over the past 3.5 decades (Dee, 2011). The spatial resolution of the data set is approximately 80 km (T255 spectral) with 60 vertical levels from the surface up to 0.1 hPa, and the grid employed is 0.75 deg resolution. ERA-Interim is produced by the European Centre for Medium-Range Weather Forecasts (ECMWF). The temporal coverage is four time steps per day. The 10-m wind product is used to estimate the wind input to the wave model, following the latest source term formulation given in Ardhuin et al. (2010).

2.3. Wave model hindcast

Wave evolution, and thus the development of a sea state, is modeled by the Radiative Transfer Equation, as follows:

$$\frac{\partial E}{\partial t} + \nabla \cdot (\vec{c_g} E) = S_{\text{wind}} - S_{\text{brk}} + S_{\text{nl}} - S_{\text{ice}}, \tag{1}$$

where $E(\omega, \theta)$ is the directional wave energy spectrum and c_g is the group velocity (Masson and LeBlond, 1989; Young, 1999). The equation describes the temporal and spatial evolution of waves as an energy budget in frequency ω and direction θ. The deep-water source/sink terms are: input from the wind S_{wind}, dissipation via breaking S_{brk}, nonlinear interactions between wave frequencies S_{nl}, and interactions with sea ice S_{ice}. This is the basis of all contemporary, i.e., third-generation, wave prediction models. Here, we use the WAVEWATCH-III model of the US National Oceanographic and Atmospheric Administration (NOAA) (Tolman, 1991, 2009) with recent improvements/options to the sea ice term S_{ice} (Rogers and Orzech, 2013) and a 16 km resolution polar stereographic grid (Rogers and Campbell, 2009) for the entire Arctic. The wave model also imports ice concentration fields from the ERA-interim, which are used to estimate the effects of sea ice on the waves using the Tolman (2003) scheme. Regions with concentration less than 25% and greater than 75% are treated as open water and land respectively. Partial blocking is applied for intermediate ice concentrations.

The wave model hindcasts are performed for the minimum ice months (August, September, and October) for whole Arctic during the years spanning 1992 to 2014. A more detailed analysis is conducted for the years 2004, 2006, 2012, 2014. These four years bracket the modern ice conditions, and include 2012 as an extreme within the 'new normal'.

Analysis of the wave model output within the defined Beaufort and Chukchi domain applies a threshold definition of ice concentrations less than 0.15 in defining "ice-free" areas. The percentage of the domain determined to be "ice-free" according to this threshold is tracked in time for each hindcast. Subsequent analyses use time series of spatial averages from the ice-free grid cells, in particular: total wave energy, $\int\int E d\theta d\omega$, the wave period at the peak of energy spectrum, T_p, and the wind stress, τ. Analyses also use histograms of the significant wave heights H_s from all ice-free grid cells and all time steps (i.e., no spatial or temporal averaging), with the conventional definition

$$\frac{1}{8}\rho g H_s^2 = \int\int E d\theta d\omega. \tag{2}$$

Finally, an evaluation of the large-scale potential of wave-ice interactions uses the normal component of wave energy flux incident to the ice-edge, given by

$$F = \int E\vec{c_g} \cdot \hat{n} d\theta, \tag{3}$$

where $\hat{n}$ is the local unit vector normal to the ice-edge. The result is the total rate at which wave energy leaves the open water and enters the sea ice (i.e., the boundary of a control volume). Figure 2 shows an example of the model hindcast and application of Eq. 3.

2.4. Satellite altimeter

Additional wave products used are from satellite altimeters: the entire Envisat record (Queffeulou and Croize-Fillon, 2012) and CRYOSAT altimetry from the NOAA Laboratory for Satellite Altimetry. The altimeter data were quality controlled and calibrated according to Zieger et al. (2009).

3. Results

3.1. Ice cover results

Trends in timing of ice advance were determined from the passive microwave record over the period 1979-2014 using the method described in Stammerjohn et al. (2012). Over this span, the timing of the autumn ice advance has become significantly later throughout the Arctic. Figure 3 shows a map of the rate of change, in days per year, for the date of the ice-edge advance. The most pronounced change has been in the Beaufort and Chukchi

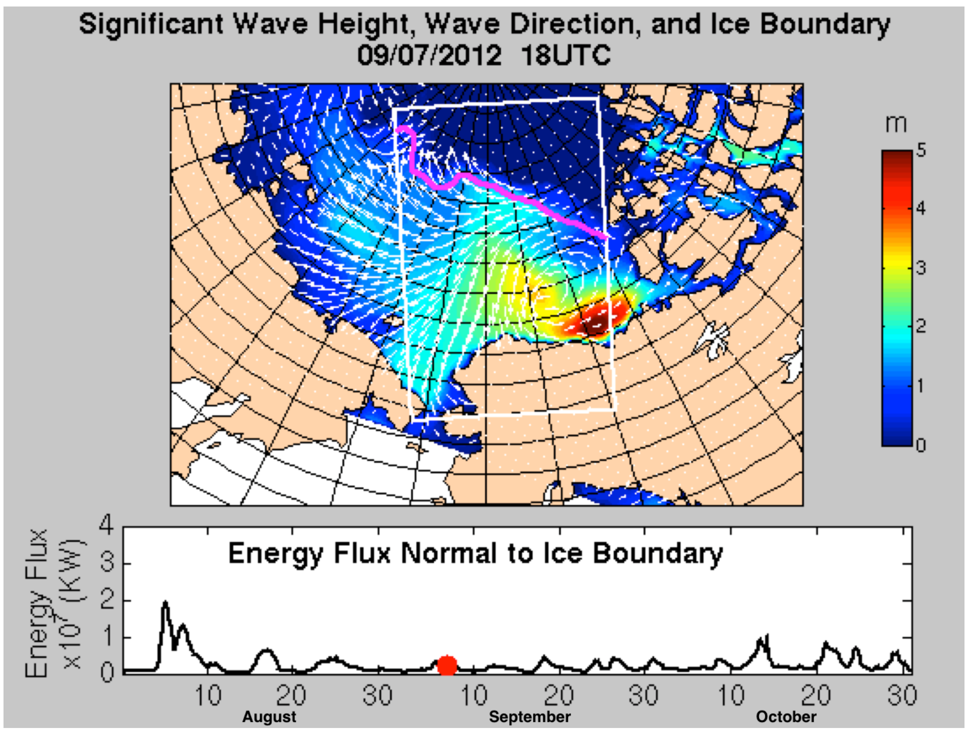

Figure 2: Example WAVEWATCH III hindcast showing significant wave heights (color scale), wave directions (white arrows), ice-edge (magenta curve), Beaufort-Chukchi domain (white outline box), and ice-normal energy flux time series (lower panel). The red dot in the lower panel corresponds to the time of the wave height map.

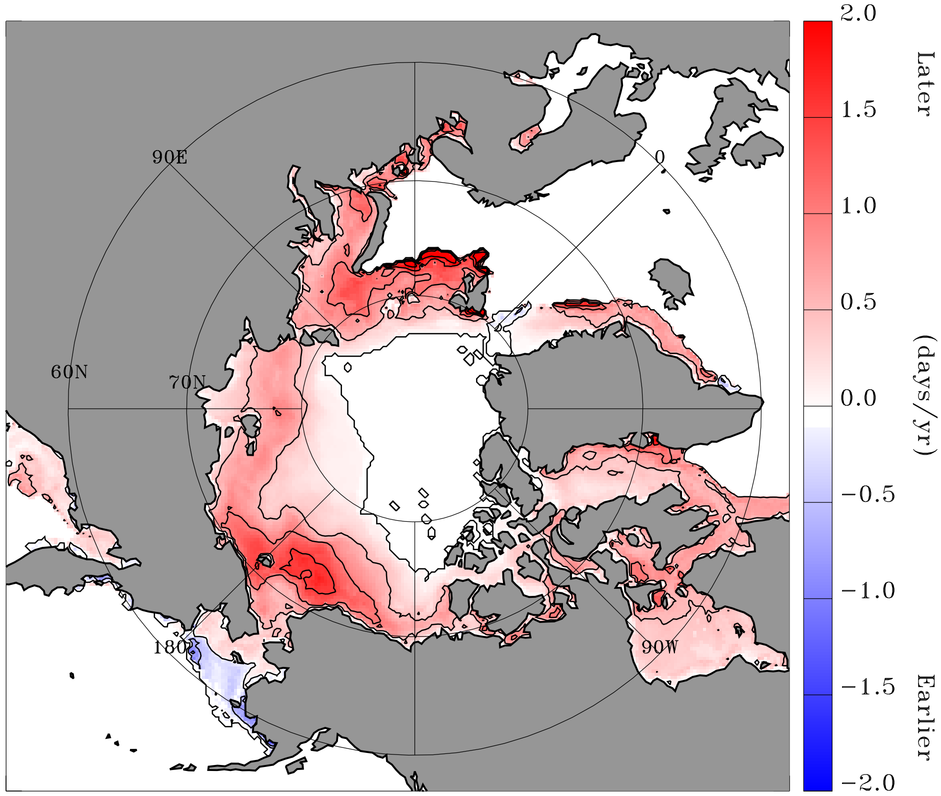

Figure 3: Average rate of change, in days per year (contours and colors), of the timing for the autumn ice advance in the Arctic. The most notable delay in ice advance is in the Beaufort and Chukchi seas (north of Alaska). Trends greater than ± 0.5 days per year are significant at the 0.01 level, with standard error determined using the effective degrees of freedom present in the regression residuals.

seas, where the statistically significant trend is 1.4 days later per year, with a similar trend towards earlier open-water in the spring. The trend is particularly strong near the northern coast of Alaska and the Chukchi shelf, where recent years have almost an additional 3 months of open water from the spring to the autumn (relative to previous decades).

The inter-annual variability of this signal is shown in Figure 4, which uses a spatial average of the ice-advance date over the defined Beaufort-Chukchi domain. The ice advance date is simply the day of the year that the ice covered portion of the domain begins to increase. The linear trend is: 0.41 ± 0.07 days per year. Note however, that the trend over the whole

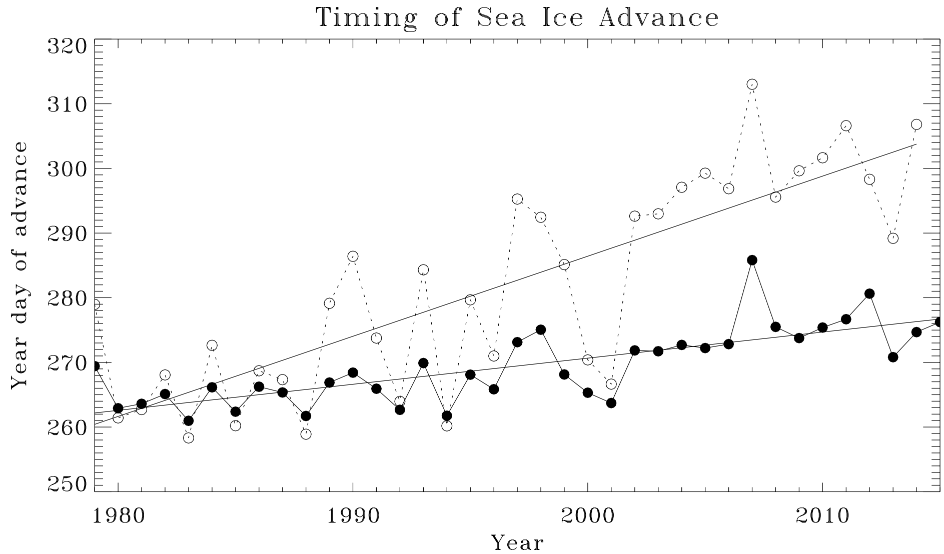

Figure 4: Spatial average for the date in the autumn when sea ice begins to refreeze and advance southwards, by year. The solid black line is the average over the entire Beaufort and Chukchi domain. The gray dashed line is the average within the coastal perimeter of the domain. The trends are shown as thin lines.

domain is modest compared with the coastal portion of the domain (where the average trend is 1.2 ± 0.2 days per year. Although 2012 was the minimum ice extent by area, 2007 is actually the latest timing for autumn ice advance in the record.

The changes in timing and ice area are likely related to the loss of multiyear ice. Ice type for the years 1999 to 2009 (using QuikSCAT) and 2008 to 2015 (using ASCAT) is shown in Figure 5. As seen, in the domain with which we are concerned, the extent of multi-year has decreased, with the most dramatic retreat in the period from 2005 to 2009. Simultaneously, the extent of the first year ice features an upward trend. Similar results can also be found in Maslanik et al. (2007, 2011). Based on satellite measurements, these authors concluded that the sea ice in the Arctic is becoming younger and thinner, represented by the extensive loss of perennial multi-year ice. Similarly, the long-term reduction in sea ice thickness in the Arctic was clearly identified by Kwok and Rothrock (2009) using a combination of submarine- and satellite-derived thickness measurements.

Both the spatial view of the overall trend (Figure 3) and the temporal view averaged over the domain (Figure 4) indicate that in recent years the

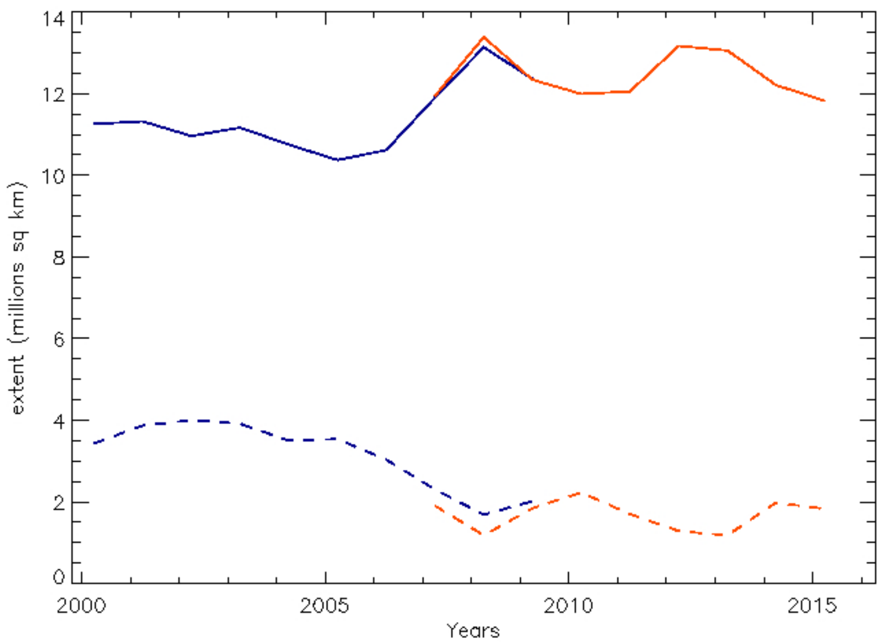

Figure 5: Multi year (solid line) and first year (dotted line) sea ice extents estimate in the Arctic for March since 2000 using satellite scatterometers. QuikSCAT sensor estimates are in blue, ASCAT results are in red (Ifremer/CERSAT).

Beaufort-Chukchi domain has more space and time with open water in the autumn. Coupled with the known pattern of strong winds in the autumn, the logical expectation is for the sea state to increase.

3.2. Sea state results

The relationship between the changing autumn ice advance and the sea state is evaluated using wave model hindcasts of the late summer and autumn from four years that span recent ice conditions. The 2004, 2006, and 2014 ice conditions are used as "typical" years, and 2012 is used as an extreme year (with minimal ice extent and delayed ice advance). This extreme year (2012) had anomalously high air and sea surface temperatures during the autumn months, and this likely contributed to the observed delay in the ice-edge advance relative to other years.

Figure 6 shows the time series of area-averaged ice and sea state quantities from these hindcasts. The percent of ice free area in the domain (panel a) is a relatively smooth quantity in time, because of area-averaging. In contrast, the sea state quantities of wave energy, peak period, and wind stress (panels b, c, and d, respectively) have high variability, because the sea state is event-driven and the autumn storms often encompass much of the domain (such that area-averaging does not smooth the signal).

The evolution of ice-free area for the four hindcast years is consistent with the timing of autumn ice advance (Figure 4), although it is interesting to note that 2006 has a similar ice-advance to 2004 and 2014, despite much less ice-free area in the late summer. The ice free area and the delay in ice advance are both notably larger for 2012 than the other years. This means more time and space were available for the generation of waves, given a set of wind forcing conditions. However, the time series of wave energy, peak period, and wind stress are not noticeably different between 2012 and the other hindcast years. Indeed, the 'Great Arctic Cyclone' of August 2012 is hardly evident in this analysis. All years show a consistent increase in winds and waves into the autumn. The largest event energy is actually from the year with the least ice-free area (2006), though it did have the strongest wind event, as described below. This event was an intense storm near the coast of Alaska, with hindcast 26 m/s maximum winds and 8 m significant wave height. This highlights the importance of wind forcing in determining the sea state, even with large variations in ice-free area. Since the area-averaged wind is not noticeably different between the different years (other than the particular storm of Oct 2006), it is not surprising that the area-averaged waves are not noticeably different.

However, the event-driven nature of the sea state is best examined probabilistically. Histograms and fitted Weibull probability distribution functions are used to identify differences, and this is where the effect of a low summer ice extent minimum followed by a late ice-edge advance in autumn in 2012 is very apparent. Using the whole domain and all time steps of the hindcasts addresses probability of a given sea state anywhere in the domain, with an explicit dependence on ice cover. Restricting the analysis to ice-free grid cells addresses the probability of a given sea state anywhere there is open water, with an implicit dependence on ice cover. In the figures that follow, results from both the whole domain and the ice-free portion are presented.

Figure 7 shows normalized histograms of significant wave heights and fitted probability distribution functions for each year using all points in the domain. The results are skewed by the high number of points with sea ice cover (and thus zero or negligible wave heights). The 2012 distribution differs from the other years, with a higher mean ($\langle H_s \rangle \sim 0.6$ m versus $\langle H_s \rangle \sim 0.3$ m) and longer tail. For example, the 2012 results have an almost 10% chance of 2 m waves at any grid cell, compared with a 1% chance of this wave height in the other years.

Figure 8 shows normalized histograms of significant wave heights and fitted probability distribution functions for each year using only ice-free points in the domain. The ice-free results across the different years are more similar than the full domain results, but 2012 still shows the largest mean and highest probability of larger waves (except in the very tail of the distributions, where limited sample sizes make differences statistically insignificant).

Figure 9 shows normalized histograms of peak wave period and fitted probability distribution functions using only ice-free points in the domain. Consistent with the results of Wang et al. (2015) and the expectations of wave maturity over larger distances, there is a shift to longer period waves for 2012. More striking, however, is the distribution for 2006, which is the year with much less ice-free area but similar ice-advance timing to 2004 and 2014. The average 2006 peak wave period is shorter and the distribution of peak wave periods is wider. This suggests that open water area may be more important han the length of the open water season in determining sea state, since the area difference for a year like 2006 persists throughout the whole season and applies to multiple storm events (whereas a delay in ice advance might only be relevant to the wave evolution of a single storm). For all years,

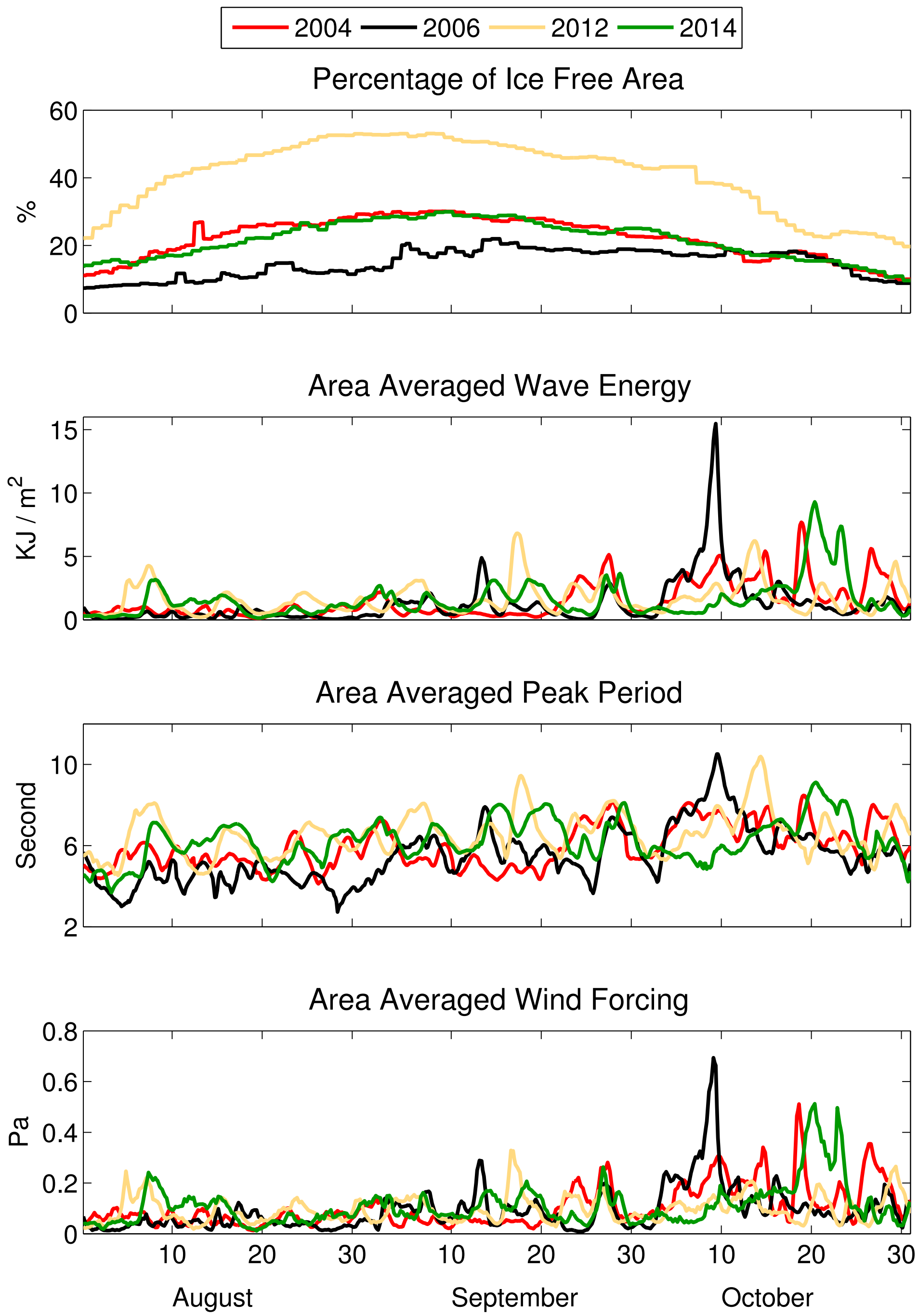

Figure 6: Time series of spatial averages over the Beaufort and Chukchi Sea in hindcasts of four selected years: (a) open water fraction, (b) wave energy, (c) wave peak period, (d) wind stress.

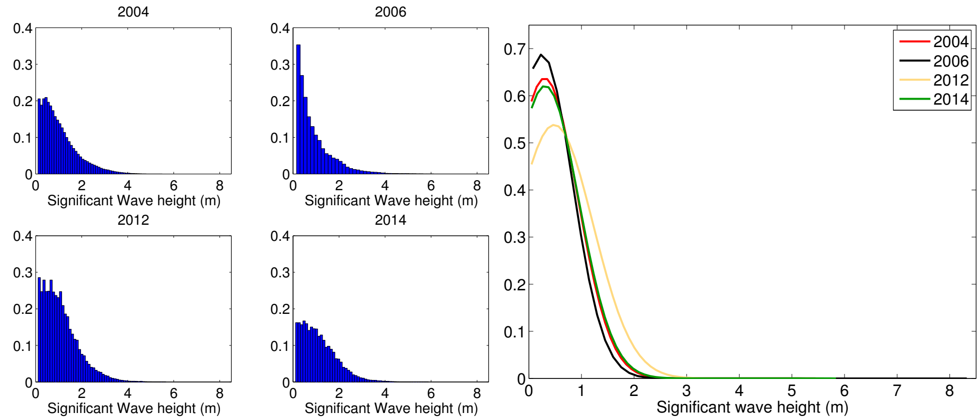

Figure 7: Normalized histograms of the significant wave height at all grid cells and all time steps for each of the hindcast years. Normalized probability distribution functions for significant wave height at all grid cells for each of the hindcast years.

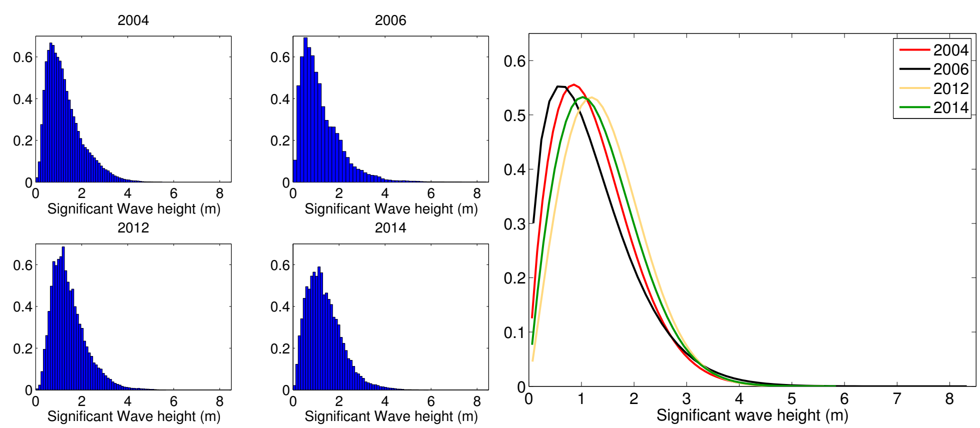

Figure 8: Normalized histograms of the significant wave height at all ice free grid cells and all time steps for each of the hindcast years. Normalized probability distribution functions for significant wave height at all ice free grid cells for each of the hindcast years.

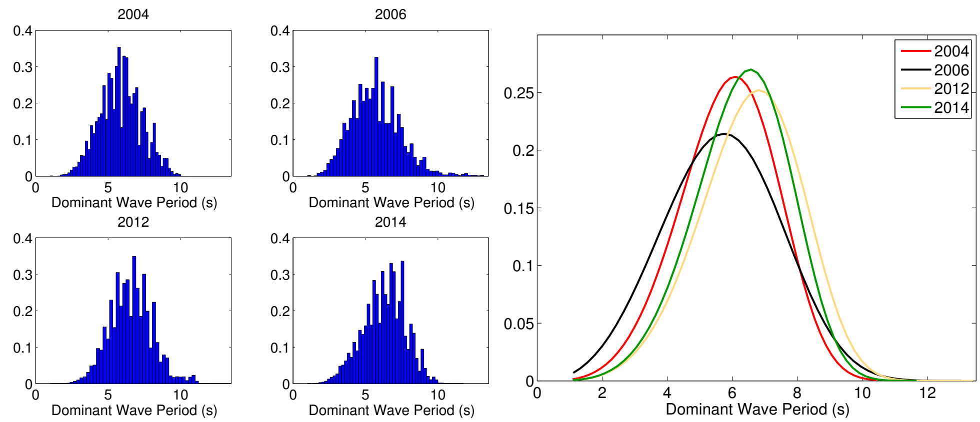

Figure 9: Normalized histograms of the peak wave period at all ice free grid cells and all time steps for each of the hindcast years. Normalized probability distribution functions for peak wave period at all ice free grid cells for each of the hindcast years.

the wave periods are still short ($T_p \sim 6$ s) relative to other oceans, indicating that, despite the emergence of swell in the Beaufort-Chukchi domain (e.g., Thomson and Rogers, 2014), the sea state of any given ice-free location in the domain is still dominated by local wind waves.

Returning to the question of wind forcing, Figure 10 shows normalized histograms of wind speed and fitted probability distribution functions using only ice-free points in the domain. Although there are minor difference in the mean wind speeds, the storm winds that drive high sea states (> 10 m/s) are not significantly different. This is consistent with Wang et al. (2015), who find that variations in wind forcing are insufficient to explain the trends in the waves.

To examine the complete signal, wave model hindcasts for every year from 1992 to 2014 are analyzed following the same fitted Weibull probability distribution function analysis used for the four years examined in detail. Figure 11 shows the Weibull scale and shape parameters for significant wave height, peak period, and wind speed. The scale is used as a proxy for the mean value and the shape is used as a proxy for the standard deviation around that mean. There are statistically significant trends at the 95% level for both wave height and peak period, but not for wind speed. The peak period signal is particularly important, since most wave-ice interaction studies have found a strong dependence of wave attenuation on wave period. Following Wadhams et al. (1988), the trends in Figure 11 imply an increasing penetration scale

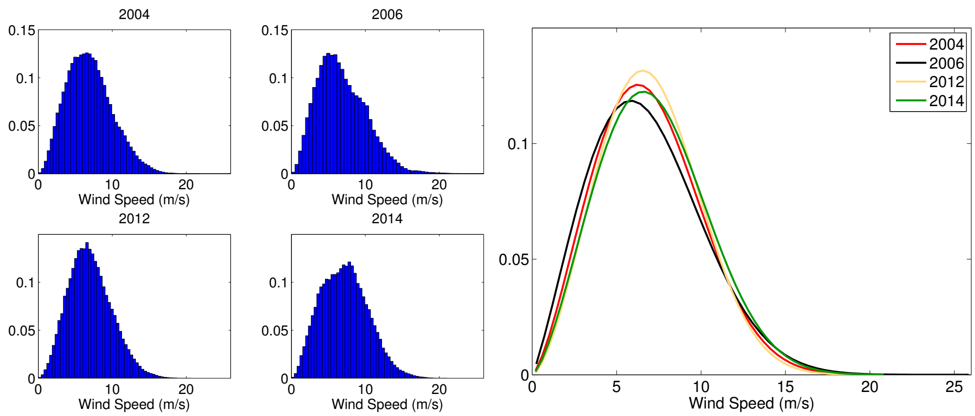

Figure 10: Normalized histograms of the wind speed at all ice free grid cells and all time steps for each of the hindcast years. Normalized probability distribution functions for wind speed at all ice free grid cells for each of the hindcast years.

for waves entering the sea ice, such that longer-period waves are expected to propagate several kilometers into the ice under recent conditions.

4. Discussion

It is logical that larger ice-free areas, which are persisting longer into the autumn, will result in higher sea states occurring more often in the Beaufort and Chukchi seas. The wave hindcasts presented here support this prediction, and the robustness of the result lies in the distinctness of the mechanism: all that is required to increase the probability of higher sea states is more ice-free area, and secondly, longer ice-free duration, not more storms or increased wind forcing. A compounding mechanism is storm duration: if storms of similar magnitude simply persist longer over open water, the resulting waves will be more mature and carry more energy flux.

The impact of an elevated autumn sea state on the overall Arctic system is difficult to determine without detailed understanding of wave-ice interactions, coastal impacts, and changes to fluxes across the air-sea-ice boundary. This is further complicated by the event-driven nature of the processes. A simplistic approach to the wave-ice question is to examine the total wave energy flux incident on the ice (Eq. 3). This is distinct from the question of overall wave activity (and associated air-sea fluxes), because an elevated sea state in the region does not affect the ice unless the waves reach the ice. Paradoxically,

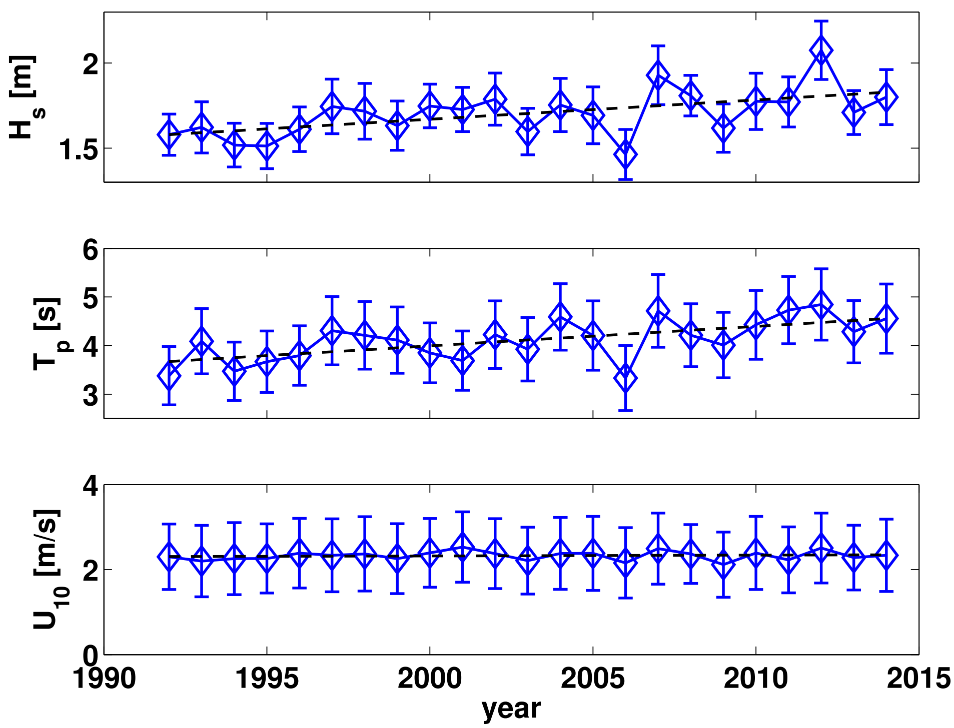

Figure 11: Trends in the Weibull fit parameters for significant wave height, peak period, and wind speed over the wave hindcast years. Diamonds are the scale parameter and the vertical bounded lines are the 95% confidence intervals of the shape parameter divided by a factor of ten (for visual simplicity). The black dashed lines are the estimated trend lines of the scale parameter. The significant wave height scale has a trend of 0.01 m increase per year and the peak period scale has a trend of 0.04 s increase per year, both of which are statistically significant at 95% confidence. The wind speed scale does not have a significant trend.

as the ice-free regions expand, there is more room for localized storms that are far from the ice and may not directly affect the ice.

Figure 12 shows time series of the total integrated wave energy flux arriving at the ice-edge. Similar to the energy results (Figure 6), the values are similar across the years and generally increase later in the autumn. This suggests that waves may be more important as a mechanism to alter ice advance (via the formation of pancakes, etc) in the autumn, rather than as a mechanism to alter ice retreat (via fracturing) in the summer. This is, of course, related to the increased ice-free area for wave generation in the autumn. The present results are inconclusive in terms of trends in wave energy flux arriving at the ice-edge. Although 2012 had more wave activity throughout the domain, the overall rate of wave energy arriving at the ice-edge was similar to other years. Still, the August 2012 storm is notable and waves may have enhanced the well-documented effect of the storm on the rest of that year (e.g., Parkinson and Comiso, 2013). Such feedbacks and the role of wave directionality are the focus of forthcoming publications, such as Stopa et al. (submitted).

Given that wave energy flux is a conserved quantity, with only minimal dissipation occurring as waves propagate in open water (e.g., Ardhuin et al., 2010), the increased wave energy inside the domain during the 2012 season can be assumed to increase the flux along the other boundary: the northern coast of Alaska. The satellite altimeter results in Figure 13 corroborate this suggestion. Figure 13 shows a statistically significant increase in wave energy along the coast from 2007 onward, compared with no significant trend (and an apparent slight decrease) in the wave energy along the ice-edge. The satellite altimeter product is scalar energy only, and thus it is not possible to calculate wave energy flux (Eq. 3) for a direct comparison and reconciliation with the wave model hindcasts. Moreover, the satellite product is not uniformly sampled and is poorly suited to the Weibull distribution fitting that was used to identify trends in the preceding sections. We thus rely on the model hindcasts for overall trends in the wave climate and discount the non-significant trend in the altimeter analysis.

This implication for increasing wave energy along the coast is significant, given the highly erodible nature of this coastline (Overeem et al., 2011). Furthermore, this would suggest that winds are preferentially directed off-ice. If so, wind-wave generation in partial ice cover may become more important in the future Arctic, when the seasonal marginal ice zone is expected to be more expansive. The process of wind-wave generation in partial ice cover is

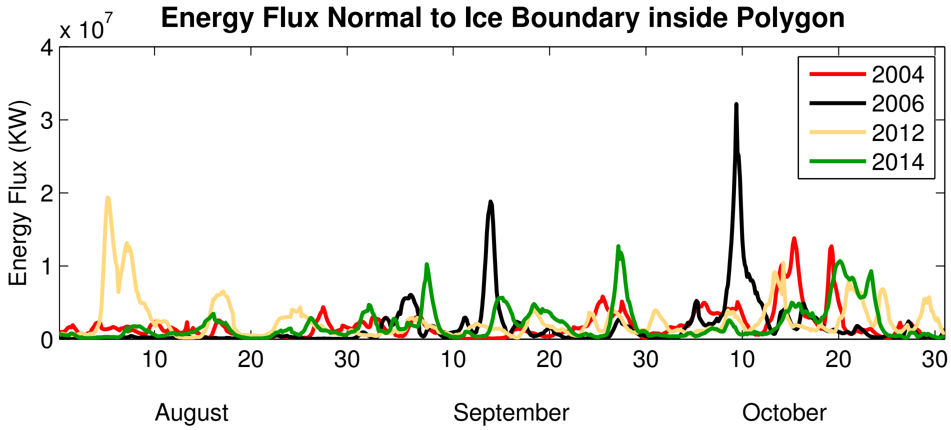

Figure 12: Time series of the total energy flux incident (normal component) to the ice-edge within the Beaufort and Chukchi seas for the hindcast years.

likely far more complex than present models suggest (Li et al., 2015; Zippel and Thomson, 2016) and is in acute need of improved understanding.

5. Conclusion

The autumn storms that regularly occur in the Beaufort and Chukchi Seas are likely elevating the sea state now, and will continue so into the future, simply because it is increasingly likely that the storms will occur over larger open water areas that persist longer into autumn. It is yet to be determined if the higher sea states will in turn feed back to the large-scale evolution of the sea ice. The increasing sea state may affect not only the ice cover development, but also wave forcing in the coastal zone. Either way, the increasing sea states may alter air-sea fluxes and associated ecosystem processes. It is possible that the increasing sea state may play an important role in modulating the presumed changes in air-sea fluxes and upper ocean properties that are occurring, and in turn may modulate the response of sea ice to climate change. Finally, higher sea states are of operational importance to mariners and seabed drilling operators in the region, for whom higher sea states can increase the likelihood of dangerous icing conditions on ships and structures.

New observational data has just been collected to assess many of these processes: the Office of Naval Research "Arctic Sea State and Boundary Layer Physics" program (Thomson et al., 2013) followed the ice-edge advance

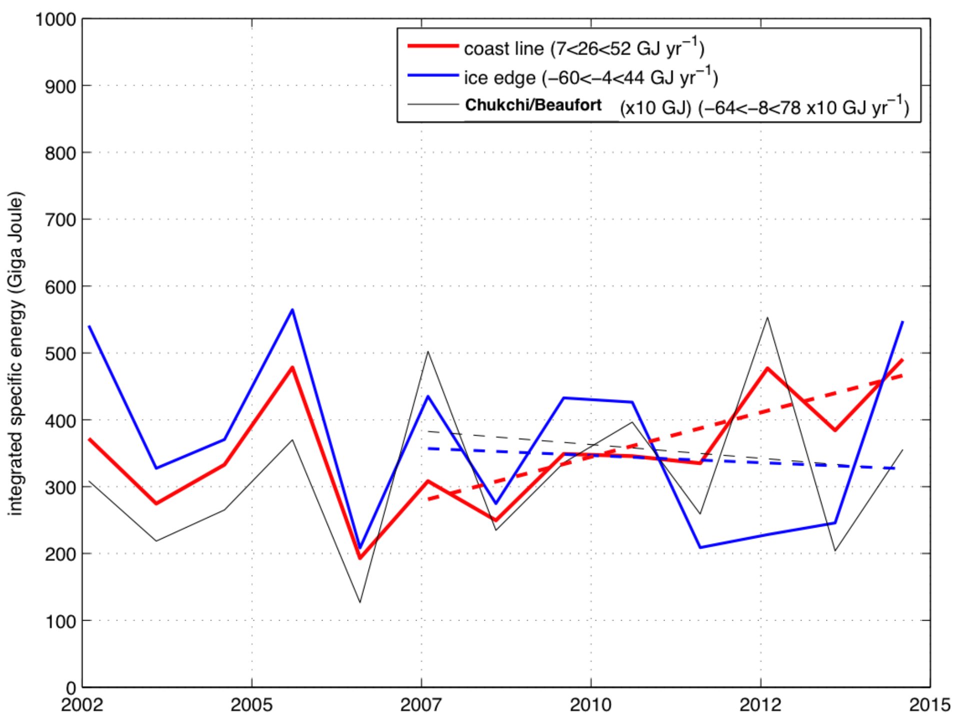

Figure 13: Yearly results from satellite altimetry estimates of spatially averaged wave energy along the northern coast of Alaska (red), along the ice-edge (blue), and over the entire domain (grey). Dashed lines show calculated trends.

during autumn 2015 while simultaneously sampling in situ air-sea-ice interactions from the R/V Sikuliaq and multiple autonomous platforms. Pancake ice associated with wave forcing was ubiquitous during the field campaign, and the importance of this ice type is assumed to be increasing with the wave climate in the region. The Sikuliaq cruise report and related information are available at http://www.apl.uw.edu/arcticseastate.

Such process studies are essential to constrain the imperfect, yet necessary, parameterizations used in climate models. Climate predictions for the Beaufort-Chukchi domain already indicate that the expansion of seasonal open water will only accelerate in the coming decades. Figure 14 shows one such example of the predicted dramatic decrease in ice volume through the autumn, using coupled ice-ocean model following the IPCC AR4 climate change scenario A1B and results from Long and Perrie (2013, 2015). These ice predictions are consistent with AR5 results following the recent work of Wang and Overland (2015). Incorporating the feedbacks associated with a changing sea state may significantly alter these predictions, but that remains a speculation until the processes can be quantified and applied within the climate models.

6. Acknowledgments

This work relies heavily on publicly available datasets, including those from the US National Snow and Ice Data Center, the Canadian Space Agency, and the European Centre for Medium-range Weather Forecasts. This work was supported by the Office of Naval Research, Code 322, “Arctic and Global Prediction”, directed by Drs. Martin Jeffries and Scott Harper. (Grant numbers and Principal Investigators are: Ackley, N000141310435; Babanin, N000141310278; Doble, N000141310290; Fairall, N0001413IP20046; Gemmrich, N000141310280; Graber, N000141310288; Guest, N0001413WX20830; Holt, N0001413IP20050; Lehner, N000141310303; Maksym, N000141310446; Rogers, N0001413WX20825; Shen, N000141310294; Squire, N000141310279; Stammerjohn, N000141310434; Thomson, N000141310284; Wadhams, N000141310289.)

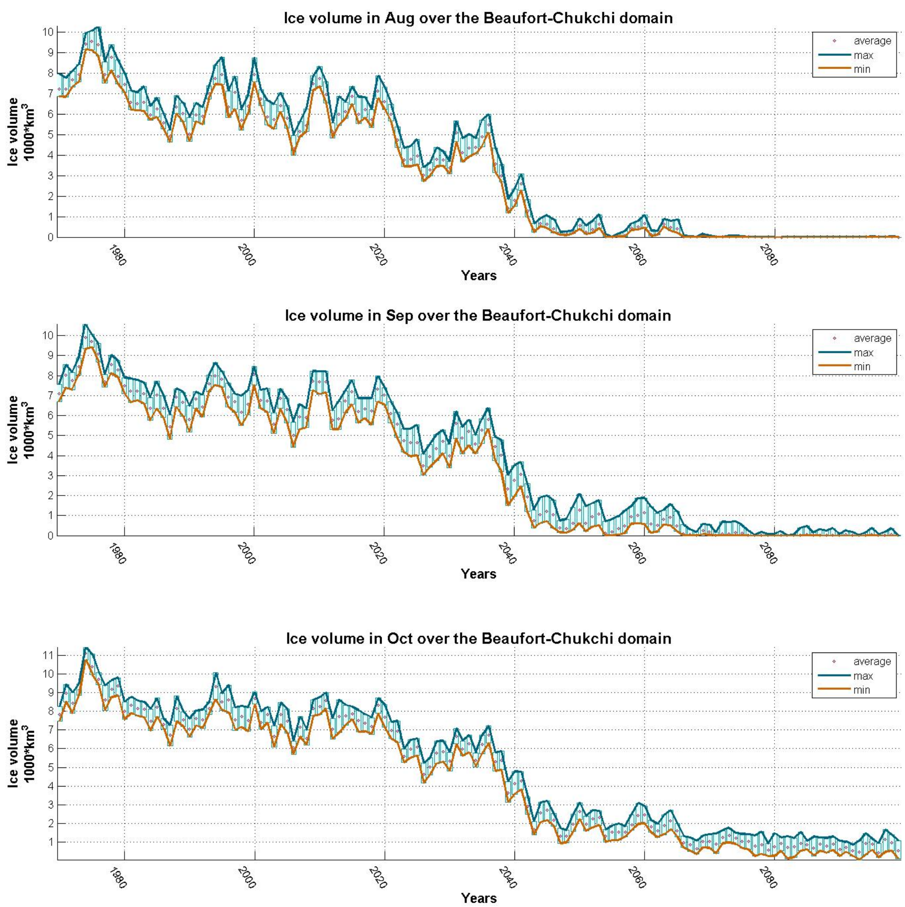

Figure 14: Estimates for ice volume in the Beaufort-Chukchi domain for 1970-2100 in the months of August, September and October using coupled ice-ocean model following the IPCC AR4 climate change scenario A1B.

References

Ardhuin, F., Rogers, W., Babanin, A., Filipot, J.-F., Magne, R., Roland, A., van der Westhuysen, A., Queffeulou, P., Lefevre, J.-M., Aouf, L., Collard, F., 2010. Semi-empirical dissipation source functions for ocean waves: Part I, definitions, calibration, and validations. J. Phys. Oceanogr. 40, 1917–1941.

Asplin, M. G., Galley, R., Barber, D. G., Prinsenberg, S., 2012. Fracture of summer perennial sea ice by ocean swell as a result of Arctic storms. J. Geophys. Res 117 (C06025).

Comiso, J. C., 2000, updated 2015. Bootstrap sea ice concentrations from Nimbus-7 SMMR and DMSP SSM/I-SSMIS. version 2. NASA National Snow and Ice Data Center Distributed Active Archive Center. http://dx.doi.org/10.5067/J6JQLS9EJ5HU.

Comiso, J. C., 2010. Polar Oceans from Space. Springer, New York.

Dee, D. P., 2011. The era-interim reanalysis: configuration and performance of the data assimilation system. Quart. J. Roy. Meteor. Soc. 137 (656), 553–597.

Francis, J. A., Vavrus, S. J., 2012. Evidence linking Arctic amplification to extreme weather in mid-latitudes. Geophysical Research Letters 39 (6), n/a–n/a.
URL `http://dx.doi.org/10.1029/2012GL051000`

Francis, O. P., Panteleev, G. G., Atkinson, D. E., 2011. Ocean wave conditions in the Chukchi Sea from satellite and in situ observations. Geophys. Res. Lett. 38 (L24610).

Girard-Ardhuin, F., Ezraty, R., 2012. Enhanced arctic sea ice drift estimation merging radiometer and scatterometer data. IEEE Trans. Geosci. Remote Sensing 50 (7), 2639–2648.

Gohin, F., Cavanie, A., 1994. A first try at identification of sea ice using the three beam scatterometer of ers-a. Int. J. Remote Sensing 15 (6), 1221–1228.

Jeffries, M. O., Overland, J. E., Perovich, D. K., 2013. The Arctic shifts to a new normal. Physics Today 66 (10).

Kwok, R., Rothrock, D. A., 2009. Decline in Arctic sea ice thickness from submarine and ICESat records: 1958–2008. Geophys. Res. Lett. 36 (L15501).

Kwok, R., Untersteiner, N., April 2011. The thinning of Arctic sea ice. Physics Today, 36–41.

Lange, M., Ackley, S., Wadhams, P., Dieckmann, G., Eicken, E., 1989. Development of sea ice in the Weddell sea. Annals of Glaciology 12.

Li, J., Kohout, A. L., Shen, H. H., 2015. Comparison of wave propagation through ice covers in calm and storm conditions. Geophysical Research Letters 42 (14), 5935–5941, 2015GL064715.
URL http://dx.doi.org/10.1002/2015GL064715

Long, Z., Perrie, W., 2013. Impacts of climate change on fresh water content and sea surface height in the Beaufort Sea. Ocean Modelling 71, 127–139.

Long, Z., Perrie, W., 2015. Scenario changes of Atlantic water in the Arctic Ocean. J. Climate 28, 552305548.

Maslanik, J. A., Fowler, C., Stroeve, J. C., Drobot, S., Zwally, J., Yi, D., Emery, W., 2007. A younger, thinner Arctic ice cover: Increased potential for rapid, extensive sea-ice loss. Geophys. Res. Lett. 34 (34).

Maslanik, J. A., Stroeve, J. C., Fowler, C., Emery, W., 2011. Distribution and trends in Arctic sea ice age through spring 2011. Geophys. Res. Lett. 38 (13), 2–7.

Masson, D., LeBlond, P., 1989. Spectral evolution of wind-generated surface gravity waves in a dispersed ice field. J. Fluid Mech. 202 (111).

Meier, W., Gallaher, D., Campbell, G. G., 2013. New estimates of Arctic and Antarctic sea ice extent during september 1964 from recovered Nimbus I satellite imagery. The Cryosphere 7, 699–705.

Overeem, I., Anderson, R. S., Wobus, C. W., Clow, G. D., Urban, F. E., Matell, N., 2011. Sea ice loss enhances wave action at the Arctic coast. Geophysical Research Letters 38 (17), n/a–n/a.
URL http://dx.doi.org/10.1029/2011GL048681

Parkinson, C. L., Comiso, J. C., 2013. On the 2012 record low Arctic sea ice cover: Combined impact of preconditioning and an August storm. Geophysical Research Letters 40, 1356–1361.

Queffeulou, P., Croize-Fillon, D., 2012. Global altimeter SWH data set. Technical Report Version 9, Laboratoire d'Oceanographie Spatiale IFREMER, Plouzanne, France.

Rogers, W., Campbell, T. J., 2009. Implementation of curvilinear coordinate system in the WAVEWATCH-III model. NRL Memorandum Report NRL/MR/7320-09-9193, Naval Research Laboratory.

Rogers, W., Orzech, M. D., 2013. Implementation and testing of ice and mud source functions in WAVEWATCH III. Memorandum Report NRL/MR/7320–13-9462, Naval Research Laboratory.
URL `http://www7320.nrlssc.navy.mil/pubs.php`

Serreze, M. C., Box, J. E., Barry, R. G., Walsh, J. E., 1993. Characteristics of Arctic synoptic activity. Met. Atmos. Phys. 51, 147–164.

Serreze, M. C., Lynch, A. H., Clark, M. P., 2001. The summer Arctic frontal zone as seen in the NCEP/NCAR reanalysis. J. Climate 14, 1550–1567.

Simmonds, I., Keay, K., 2009. Extraordinary September arctic sea ice reductions and their relationships with storm behavior over 1979-2008. Geophys. Res. Lett.. 36 (L19715).

Simmonds, I. K., Keay, K., 2012. The great Arctic cyclone of August 2012. Geophys. Res. Lett. 39 (L23709).

Squire, V. A., 2007. Of ocean waves and sea ice revisited. Cold Regions Sci. Tech. 49, 110–133.

Squire, V. A., Dugan, J. P., Wadhams, P., Rottier, P. J., Liu, A. K., 1995. Of ocean waves and sea ice. Annu. Rev. Fluid Mech. 27, 115–168.

Stammerjohn, S., Massom, R., Rind, D., Martinson, D., 2012. Regions of rapid sea ice change: An inter-hemispheric seasonal comparison. Geophysical Research Letters 39 (6), n/a–n/a, l06501.
URL `http://dx.doi.org/10.1029/2012GL050874`

Stopa, J. E., Ardhuin, F., Girard-Adrhuin, F., submitted. Wave-climate in the Arctic 1992-2014: seasonality, trends, and wave-ice influence. The Cryosphere.

Stroeve, J., Serreze, M., Drobot, S., Gearheard, S., Holland, M., et al., 2008. Arctic sea ice extent plummets in 2007. Eos Trans. AGU 89, 1314.

Stroeve, J. C., Serreze, M. C., Fetterer, F., Arbetter, T., Meier, W., 2005. Tracking the Arctic's shrinking ice cover: Another extreme September minimum in 2004. Geophys. Res. Let. 32 (L04501).

Thomson, J., Rogers, W. E., 2014. Swell and sea in the emerging Arctic Ocean. Geophysical Research Letters, n/a–n/a.
URL `http://dx.doi.org/10.1002/2014GL059983`

Thomson, J., Squire, V., Ackley, S., Rogers, E., Babanin, A., Guest, P., Maksym, T., Wadhams, P., Stammerjohn, S., Fairall, C., Persson, O., Doble, M., Graber, H., Shen, H., Gemmrich, J., Lehner, S., Holt, B., Williams, T., Meylan, M., Bidlot, J., 2013. Science plan: Sea state and boundary layer physics of the emerging Arctic Ocean. Technical Report 1306, Applied Physics Laboratory, University of Washington.

Tolman, H. L., 1991. A third generation model for wind-waves on slowly varying, unsteady, and inhomogeneous depths and currents. J. Phys. Oceanogr. 21 (6), 782–797.

Tolman, H. L., 2003. Treatment of unresolved islands and ice in wind wave models. Ocean Modeling 5, 219–231.

Tolman, H. L., 2009. User manual and system documentation of WAVEWATCH III version 3.14. Tech. Rep. 276, NOAA/NWS/NCEP/Marine Modeling and Analysis Branc, Camp Springs, MD (USA).

Tran, N., Girard-Adrhuin, F., Ezraty, R., Feng, H., Femenias, P., January 2009. Defining a sea ice flag for Envisat altimetry mission. IEEE Geoscience and Remote Sensing Letters 6 (1), 77–81.

Vermaire, J. C., Pisaric, M. F. J., Thienpont, J. R., Courtney Mustaphi, C. J., Kokelj, S. V., Smol, J. P., 2013. Arctic climate warming and sea ice declines lead to increased storm surge activity. Geophysical Research

Letters 40 (7), 1386–1390.
URL http://dx.doi.org/10.1002/grl.50191

Wadhams, P., 1990. Evidence for thinning of the Arctic ice cover north of Greenland. Nature 345 (795-797).

Wadhams, P., Davis, N. R., 2000. Further evidence of ice thinning in the Arctic Ocean. Geophys. Res. Lett. 27 (24), 3973–3976.

Wadhams, P., Lange, M. A., Ackley, S. F., 1987. The ice thickness distribution across the Atlantic sector of the Antarctic Ocean in midwinter. J. Geophys. Res 92 (C13), 14535–14552.

Wadhams, P., Squire, V. A., Goodman, D. J., Cowan, A. M., Moore, S. C., 1988. The attenuation rates of ocean waves in the marginal ice zone. J. Geophys. Res 93 (C6), 6799–6818.

Wang, M., Overland, J., January 2015. Projected future duration of the sea-ice-free season in the Alaskan Arctic. Progress in Oceanography.

Wang, X. L., Feng, Y., Swail, V. R., Cox, A., 2015/08/28 2015. Historical changes in the Beaufort-Chukchi-Bering seas surface winds and waves, 1971-2013. Journal of Climate.
URL http://dx.doi.org/10.1175/JCLI-D-15-0190.1

Young, I., 1999. Wind Generated Ocean Waves. Elsevier Ocean Engineering Book Series. Elsevier, New York.

Zhang, J., Lindsay, R., Schweiger, A., Steele, M., 2013. The impact of an intense summer cyclone on 2012 Arctic sea ice retreat. Geophysical Research Letters 40 (4), 720–726.
URL http://dx.doi.org/10.1002/grl.50190

Zhang, X., Walsh, J., Zhang, J., Bhatt, U., Ikeda, M., 2004. Climatology and interannual variability of Arctic cyclone activity: 1948-2002,. J. Climate 17, 2300–2317.

Zieger, S., Vinoth, J., Young, I. R., 2009. Joint calibration of multi-platform altimeter measurements of wind speed and wave height over the past 20 years. J. Atmos. Ocean. Tech. 26, 2549–2564.

Zippel, S., Thomson, J., 2016. Air-sea interactions in the marginal ice zone. Elementa.